11-2002

Hybrid Two-Dimensional Finite Element Model of Tires

Yong Joe Kim
Purdue University

J Stuart Bolton
Purdue University, bolton@purdue.edu

타이어의 복합 이차원 유한 요소 모델

Hybrid Two-Dimensional Finite Element Model of Tires

김용조*·J. Stuart Bolton**

Yong-Joe Kim and J. Stuart Bolton

Key Words: tire, hybrid finite element, dispersion relation, waveguide

ABSTRACT

It has been shown that the vibrational response of a tire can be represented by a set of decaying waves, each associated with a particular cross-sectional mode shape in the region near the contact patch. Thus, it can be concluded that tires can be effectively modeled as lossy waveguides. It has also been shown that the sound radiation from tires is mainly from the region close to the contact patch. In consequence, it may be computationally efficient to analyze tire vibration and sound radiation in the region close to the contact patch by using a hybrid finite element model in which the cross-section of a tire is approximated by 2-D finite elements while an analytical wave solution is assumed in the circumferential direction of the tire. In this article, a hybrid finite element was formulated based on a composite shell model. The dispersion relations for sample structures obtained by using the hybrid FE model were then compared with those obtained by using a full, three-dimensional FE model. It has been shown that the FE analysis made using the hybrid 2-D finite elements yields results in close agreement with the three-dimensional model.

1. Introduction

Automobile noise is one of the most annoying environmental noise problems since the number of automobiles has increased dramatically over the last few decades. It is well known that tire/road noise is a major contributor to exterior automobile noise: the other types of noise generated by an automobile such as engine noise, muffler noise, aerodynamic noise, and so on, can be relatively easily controlled since various noise control techniques directed at those sources have been successfully developed. Among the numerous possible tire noise mechanisms, tire vibration has been extensively investigated as a primary noise source.

In earlier experimental work, a stationary tire was driven radially at a point on its treadband and measurements of the resulting radial treadband vibration were made around the treadband circumference by using a laser Doppler velocimeter. By performing a circumferential wave number transform of the measured space-frequency data, the wave propagation characteristics of a tire could be visualized [1]. In an attempt to understand these experimental results in details, the tire treadband was modeled as a circular cylindrical shell with air pressure acting on its interior surface [2,3]. To identify effects of tire rotation on wave propagation, rotation of a circular cylindrical shell was also considered [3]. This shell model was found to explain the principal wave propagation characteristics of a tire: i.e., the vibrational response of a tire can be expressed as a superposition of decaying waves, each associated with a particular cross-sectional mode shape. Thus, it can be concluded that a tire can be modeled as a lossy waveguide [1-3].

When a FE model of a tire is used to analyze tire vibration at high frequencies, the size of the elements should be small and the tire's cross-section should be modeled in detail since the wavelength may be comparable to the thickness of the tire. In consequence, a full, 3-D finite element model for high frequency analysis may require tremendous modeling efforts and computational resources.

Since tires behave like constant cross-section waveguides, it would be computationally efficient to analyze tire vibration by using hybrid, 2-D FE models: i.e., the cross-section of a tire is approximated by finite elements while a propagating wave solution is assumed in the circumferential direction.

Previously, Cheung [4] described a hybrid, 2-D FE formulation based on the use of strip elements: shape functions are prescribed in the cross-sectional direction and analytical mode shapes in the axial direction. Richards [5] analyzed the vibrational response of a tire coupled with an internal acoustical cavity by applying hybrid 2-D finite elements to both the tire and acoustical cavity. In his case, the tire was modeled as a membrane. In addition, Brockman et al. [6] have estimated tire critical speeds by using a hybrid 2-D FE model. They used solid elements in cylindrical coordinates and considered the tires' rotation in the circumferential direction; inflation pressure was also considered. Nilsson and Finnveden [7] calculated the input point mobility of a tire by using a hybrid 2-D FE model based on orthotropic, pre-stressed conical shell elements.

Here, a hybrid 2-D finite element for a composite shell with finite curvature was derived. As a first step in the application of the hybrid 2-D finite element, a tire was

modeled as a finite, orthotropic circular cylindrical shell. Natural frequencies and mode shapes were then calculated and dispersion relations were obtained. A full, 3-D FE model that had the same geometry and material properties as the hybrid 2-D model was implemented for the purpose of comparison.

2. Derivation of Composite Shell Element

2.1 Displacement and Strain

Here, we define the 1- and 2-directions as tangential to shell surface and the 3-direction as normal to shell surface. It is assumed that vibrational displacements of a shell can be approximated by shape functions in the 1-direction and represented by an analytical solution in the 2-direction. Consider a finite element, on the shell, that has two nodal lines in the 2-direction. Then, the displacement vector $\mathbf{u} = [u_1\ u_2\ u_3]^T$ of the element can be expressed as

$$\mathbf{u}(x_1, x_2, t) = \boldsymbol{\chi}(x_1)\mathbf{y}(t, x_2), \tag{1}$$

where $\boldsymbol{\chi}$ is the matrix of shape functions (see Appendix A) and $\mathbf{y}$ is the nodal displacement vector. The nodal displacement vector is defined as $\mathbf{y} = [u_{11}\ u_{21}\ u_{12}\ u_{22}\ u_{13}\ \beta_{11}\ u_{23}\ \beta_{21}]^T$, where u_{mn} is the translational displacement in the n-direction at the m-th node and β_{mn} is the rotational displacement in the n-direction at the m-th node. Note that an element has two nodes and that each node has four nodal displacements (three translational displacements and one rotational displacement) that are functions of t and x_2.

When the shear deformation of the shell is assumed to be negligible, strain can be separated into membrane and bending strains. These strains can be directly related to displacements (see Appendix B). By substituting Eq. (1) into the strain-displacement relations, strains can then be associated with the nodal displacement vector: i.e.,

$$\boldsymbol{\varepsilon} = \mathbf{E}_0\mathbf{y} + \mathbf{E}_1\frac{\partial \mathbf{y}}{\partial x_2} + \mathbf{E}_2\frac{\partial^2 \mathbf{y}}{\partial x_2^2}, \tag{2}$$

where $\boldsymbol{\varepsilon}$ is the strain vector, $\boldsymbol{\varepsilon} = [\varepsilon_{11}\ \varepsilon_{22}\ \varepsilon_{12}\ \kappa_{11}\ \kappa_{22}\ \kappa_{12}]^T$, ε_{mn} is the membrane strain and κ_{mn} is the bending strain.

2.2 Energy Expressions for the Composite Shell

For a composite shell, the resultant forces obtained by integrating the stresses in the thickness direction (x_3) can be related to the strains: i.e.,

$$\mathbf{R} = \mathbf{C}\boldsymbol{\varepsilon}, \tag{3}$$

where $\mathbf{R} = [N_{11}\ N_{22}\ N_{12}\ M_{11}\ M_{22}\ M_{12}]^T$ is the resultant force vector. The resultant forces and moments are expressed as

$$N_{mn} = \int_{-h/2}^{h/2} \sigma_{mn}\, dx_3$$

and

$$M_{mn} = \int_{-h/2}^{h/2} x_3\sigma_{mn}\, dx_3,$$

where σ_{mn} is the stress and h is the thickness of the shell.

The potential energy stored in the element can be expressed in terms of the strain vector by making use of Eq. (3): i.e.,

$$\begin{aligned} U &= \frac{1}{2}\int_{t_0}^{t_1}\int_{x_1}\int_{x_2} \left(\mathbf{R}^T\boldsymbol{\varepsilon}\right) A_1A_2\, dx_1dx_2dt \\ &= \frac{1}{2}\int_{t_0}^{t_1}\int_{x_1}\int_{x_2} \left(\boldsymbol{\varepsilon}^T\mathbf{C}^T\boldsymbol{\varepsilon}\right) A_1A_2\, dx_1dx_2dt \end{aligned}, \tag{3}$$

where A_m (m = 1,2) is the Lamé parameter of the shell. The kinetic energy can be expressed as

$$T = \frac{1}{2}\int_{t_0}^{t_1}\int_{x_1}\int_{x_2} \rho h\left(\dot{\mathbf{y}}^T\boldsymbol{\chi}^T\boldsymbol{\chi}\dot{\mathbf{y}}\right) A_1A_2\, dx_1dx_2dt, \tag{4}$$

where ρ is the density averaged over the element thickness, h. Finally, consider the work done by external forces. The work done by distributed forces is

$$W_q = \int_{t_0}^{t_1}\int_{x_1}\int_{x_2} \left(\mathbf{y}^T\boldsymbol{\chi}^T\mathbf{Q}^e\right) A_1A_2\, dx_1dx_2dt \tag{5}$$

and the work done by point forces applied at the nodes is

$$W_f = \int_{t_0}^{t_1}\int_{x_2} \left(\mathbf{y}^T\mathbf{F}^e\right) A_2\, dx_2dt, \tag{6}$$

where $\mathbf{Q}^e = [q_1\ q_2\ q_3]^T$ is the distributed force vector and $\mathbf{F}^e = [F_{11}\ F_{21}\ F_{12}\ F_{22}\ F_{13}\ F_{14}\ F_{23}\ F_{24}]^T$ is the external, nodal force vector (see Appendix C).

2.3 Variational Principle

The element equation can be obtained by taking a small variation of the nodal displacements in the energy expression: i.e.,

$$\delta\left(U - T - W_q - W_f\right) = 0. \tag{7}$$

By substituting Eqs. (3) to (6) into Eq. (7), the system equation for one element can be derived as

$$\sum_{m=0}^{4}\mathbf{K}_m\frac{\partial^m \mathbf{y}}{\partial x_2^m} + \mathbf{M}\ddot{\mathbf{y}} = \mathbf{F}^e + \mathbf{F}^i + \mathbf{Q}, \tag{8}$$

where $\mathbf{K}_m$ is the m-th stiffness matrix, $\mathbf{M}$ is the mass matrix, $\mathbf{F}^i$ is the internal, nodal force vector, and $\mathbf{Q} = [Q_{11}\ Q_{21}\ Q_{12}\ Q_{22}\ Q_{13}\ Q_{14}\ Q_{23}\ Q_{24}]^T$ is the generalized, distributed force vector (see Appendix C). When more than one element is used for the analysis of a system, a

global system equation can be assembled from the individual element equations by applying conditions of displacement continuity and force balance at each node.

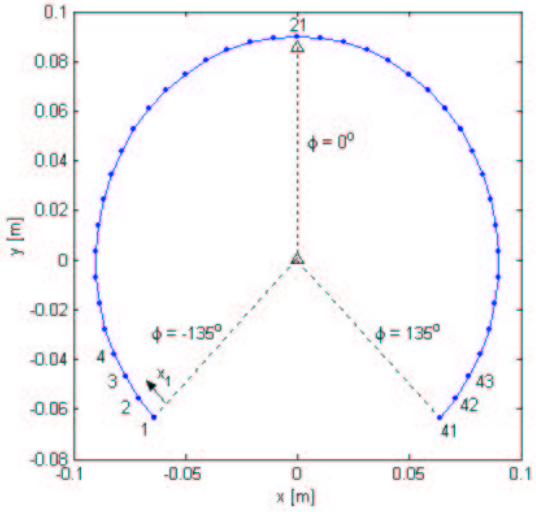

Fig. 1 Hybrid 2-D FE model of circular cylindrical shell: dots represent nodes and solid lines indicate finite elements.

Table 1 List of parameters used for tire models.

Young's Moduli	$E_1 = 3.2\times10^8$ Pa $E_2 = 7.5\times10^8$ Pa
Shear Modulus	$G_{12} = 5.0\times10^7$ Pa
Poisson's Ratio	$\nu_{12} = 0.45$
Density	1200 kg/m^3
Thickness	$h = 0.008$ m

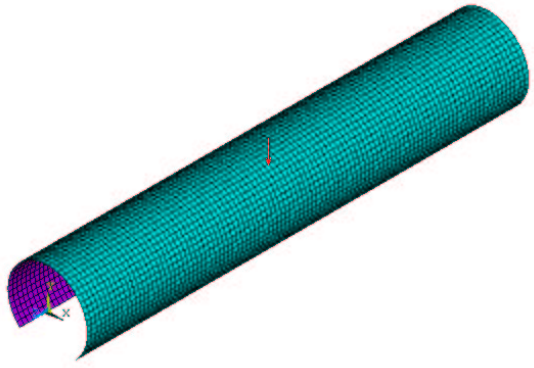

Fig. 2 Full, 3-D finite element model of incomplete, orthotropic circular cylindrical shell implanted in ANSYS version 5.7. Arrow at the center indicates point input force.

3. Tire Models

Keltie [8] obtained analytical solutions for the vibrational response and sound radiation in the case of an infinite, isotropic, circular cylindrical shell model of a tire.

Here, tires are modeled as an orthotropic circular cylindrical shell by using both hybrid, 2-D finite elements and full, 3-D finite elements. It is thus assumed that the radius of curvature in the cross-sectional direction (x_1) is constant and the radius of curvature in the circumferential direction (x_2) is infinite: i.e., at relatively high frequencies, the radius of curvature in the 2-direction is much larger than the vibrational wavelength. It is also assumed that the thickness of the shell is constant and a single material is used for both sidewall and treadband. The tire parameters are listed in Table 1: they were adapted from the literature [10], were based on physical reasoning, or were obtained by direct measurement of tires. The translational displacements at the edges of tire's sidewall were set to zero.

3.1 2-D FE Model

As an application of the hybrid, 2-D finite element derived in the previous section, the cross-section of a tire was modeled by using 40 finite elements as shown in Fig. 1. The radius of the cross-section was 0.09 m and the radius of curvature in the 2-direction was infinite. It is assumed that within an element the radius of curvature in the 1-direction is infinite. Since the radius of curvature in the 2-direction is infinite, the finite elements used in model were plate-like with $A_1 = 1$, $A_2 = 1$, $R_1 = 0$, and $R_2 = 0$. Note that top node (node number 21) in Fig. 1 is located at $\phi = 0°$, the first node (node number 1) at $\phi = -135°$, and the last node (node number 41) at $\phi = 135°$.

The global system equation obtained after the matrix assembly process is the partial differential system equation that includes a fourth order spatial derivative (in the 2-direction) and a second order time derivative. To solve this system equation, a natural vibration problem without damping and external force should be solved first (in this article, only the natural vibration analysis of the hybrid 2-D FE model will be considered). When simply supported boundary conditions are applied at both ends of the circular cylinder, the nodal solutions can be assumed to have the form

$$\mathbf{y}_n(t, x_2) = \mathbf{Y}_n \exp(ik_2 x_2)\exp(-i\omega_n t), \qquad (9)$$

where $k_2 = n\pi/L$ is the wave number in the 2-direction, L is the length of the circular cylinder, and n is the mode number in the 2-direction (n is an integer number). By substituting Eq. (9) into the homogeneous, global system equation, an eigenvalue problem is derived as

$$\left[\sum_{m=0}^{4}\left(\frac{in\pi}{L}\right)^{m}\mathbf{K}_{m}-\omega_{n}^{2}\mathbf{M}\right]\mathbf{Y}_{n}=\mathbf{0}. \qquad (10)$$

The natural frequencies, ω_n, and mode shapes, $\mathbf{Y}_n$, can be calculated from Eq. (10) for a given n.

3.2 Full, 3-D FE Model

The FE mesh and location of the applied force are shown in Fig. 2. ANSYS element type SHELL63 was used to represent the tire: there were 40 elements in the 1-direction and 100 elements in the 2-direction. Simply supported boundary conditions were imposed at $x_2 = 0$ and $x_2 = L$. The point force was applied at $\phi = 0$ and $x_2 = L/2$. The resulting vibrational velocities were recorded along the nodes at $\phi = 0$. Then the spatially distributed velocity data at each frequency was transformed into a wave number spectrum by applying the spatial Fourier transform: i.e., frequency-space domain data was transformed into frequency-wave number domain data [1].

3.3 Results and Discussion

Figure 3(a) shows the frequency-wave number spectrum of the vibrational responses obtained from the full, 3-D FE analysis. The results of Fig. 3(a) were re-plotted in Fig. 3(b) along with the dispersion relations (indicated by dots) which are the relations between the natural frequencies, ω_n, obtained from Eq. (10), and the wave numbers ($k_2 = n\pi/L$). In Fig. 3(b), two solid lines at $n = 11$ and $n = 20$ are also shown. In Figs. 4 and 5, the first four displacement mode shapes (from the lowest natural frequency) in the 3-direction (normal to the shell surface) are shown along with their natural frequencies when $n = 11$ and $n = 20$, respectively.

The frequency-wave number domain results are symmetrical with respect to the zero wave number axis, indicating that waves propagate equally in the positive and negative directions (see Fig. 3).

In Fig. 3(a), there are at least four visible curving trajectories below 1200 Hz indicating the existence of at least four wave modes propagating in the 2-direction. Actually, there are more than four propagating wave types possible in this case: they can be identified from the dispersion relations obtained from the natural vibration analysis of the hybrid, 2-D FE model (see Fig. 3(b)). However, only the four wave types whose cross-sectional mode shape does not have a node at the center of the treadband were excited since the point force was applied at the center: e.g., the second and third cross-sectional modes in Figs. 4 and 5 are driven but the first and fourth are not. When we compare Figs. 4 and 5, the first three cross-sectional mode shapes are almost identical which means that each curving trajectory is associated with a particular cross-sectional mode shape that is only slightly frequency-dependent.

4. Conclusions

In this article, a hybrid 2-D finite element for a composite shell was formulated by using the variational principle. For the purpose of validating the hybrid 2-D finite element, a finite, orthotropic circular cylindrical shell model of a tire was analyzed by using both hybrid 2-D plate finite elements and full, 3-D finite elements. Although here natural vibration was analyzed by using a hybrid 2-D FE model and forced vibration by using a full, 3-D FE model, both models could be used in either role. A forced 2-D model will be developed in future work.

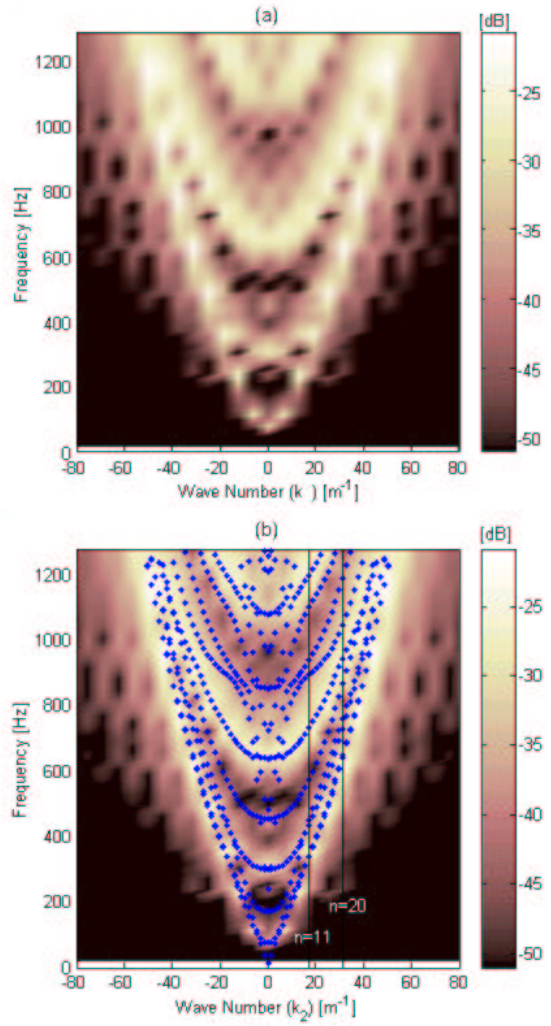

Fig. 3 (a) Frequency-wave number domain representation of the forced responses obtained from full, 3-D FE analysis and (b) dispersion relations (dots) obtained from hybrid 2-D FE analysis overlaid on forced responses (contour) presented in Fig 3(a).

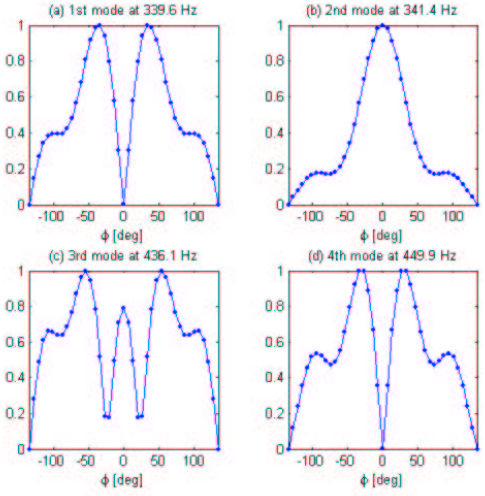

Fig. 4 Natural displacement mode shapes in the 3-direction and associated natural frequencies obtained from hybrid 2-D FE analysis when n = 11.

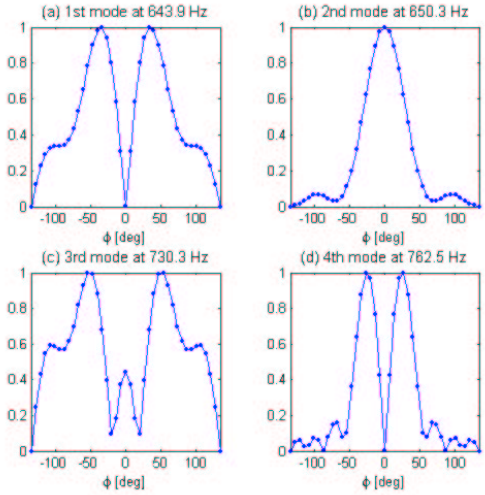

Fig. 5 Natural displacement mode shapes in the 3-direction and associated natural frequencies obtained from hybrid 2-D FE analysis when n = 20.

Appendix A

Displacements in the 1- and 2-directions are represented by a first order polynomial while the displacement in the 3-direction is represented by a third order polynomial that is normally used for beam elements: i.e.,

$$u_1 = \chi_{11}u_{11} + \chi_{21}u_{21}, \tag{A1}$$

$$u_2 = \chi_{12}u_{12} + \chi_{22}u_{22}, \tag{A2}$$

and

$$u_3 = \chi_{13}u_{13} + \chi_{14}\theta_{11} + \chi_{23}u_{23} + \chi_{24}\theta_{21}, \tag{A3}$$

where the first index of χ and u on the right-hand side indicates node number and the second index denotes the direction of displacement. When the two nodes of a element are located at x_1 = -1 and x_1 = 1, the shape functions are

$$\chi_{11} = 1/2(1-x_1), \tag{A4}$$

$$\chi_{21} = 1/2(1+x_1), \tag{A5}$$

$$\chi_{12} = \chi_{11}, \tag{A6}$$

$$\chi_{22} = \chi_{21}, \tag{A7}$$

$$\chi_{13} = 1-3[(1+x_1)/2]^2 + 2[(1+x_1)/2]^3, \tag{A8}$$

$$\chi_{14} = -(1+x_1)[1-(1+x_1)/2]^2, \tag{A9}$$

$$\chi_{23} = 3[(1+x_1)/2]^2 - 2[(1+x_1)/2]^3, \tag{A10}$$

and

$$\chi_{24} = (1+x_1)[\{(1+x_1)/2\}^2 - (1+x_1)/2]. \tag{A11}$$

Appendix B

Expressions for the strains of thin shells were derived by Soedel [9] and they are presented here for completeness. They can be separated in terms of membrane strains and bending strains: i.e.,

$$\varepsilon_{11} = \varepsilon_{11}^0 + x_3\kappa_{11}, \tag{B1}$$

$$\varepsilon_{22} = \varepsilon_{22}^0 + x_3\kappa_{22}, \tag{B2}$$

and

$$\varepsilon_{12} = \varepsilon_{12}^0 + x_3\kappa_{12}, \tag{B3}$$

where the membrane strains are

$$\varepsilon_{11}^0 = \frac{1}{A_1}\frac{\partial u_1}{\partial x_1} + \frac{u_2}{A_1A_2}\frac{\partial A_1}{\partial x_2} + \frac{u_3}{R_1}, \tag{B4}$$

$$\varepsilon_{22}^0 = \frac{1}{A_2}\frac{\partial u_2}{\partial x_2} + \frac{u_1}{A_1A_2}\frac{\partial A_2}{\partial x_1} + \frac{u_3}{R_2}, \tag{B5}$$

$$\varepsilon_{12}^0 = \frac{A_2}{A_1}\frac{\partial}{\partial x_1}\left(\frac{u_2}{A_2}\right) + \frac{A_1}{A_2}\frac{\partial}{\partial x_2}\left(\frac{u_1}{A_1}\right), \tag{B6}$$

the bending strains are

$$\kappa_{11} = \frac{1}{A_1}\frac{\partial \beta_1}{\partial x_1} + \frac{\beta_2}{A_1A_2}\frac{\partial A_1}{\partial x_2}, \tag{B4}$$

$$\kappa_{22} = \frac{1}{A_2}\frac{\partial \beta_2}{\partial x_2} + \frac{\beta_1}{A_1 A_2}\frac{\partial A_2}{\partial x_1}, \tag{B5}$$

$$\kappa_{12} = \frac{A_2}{A_1}\frac{\partial}{\partial x_1}\left(\frac{\theta_2}{A_2}\right) + \frac{A_1}{A_2}\frac{\partial}{\partial x_2}\left(\frac{\theta_1}{A_1}\right), \tag{B6}$$

and the rotational displacements are

$$\beta_1 = \frac{u_1}{R_1} - \frac{1}{A_1}\frac{\partial u_3}{\partial x_1}, \tag{B7}$$

and

$$\beta_2 = \frac{u_2}{R_2} - \frac{1}{A_2}\frac{\partial u_3}{\partial x_2}, \tag{B8}$$

where R_m is the radius of curvature in the m-direction.

Appendix C

Stiffness matrices are represented in terms of matrices, $\mathbf{E}_0$, $\mathbf{E}_1$, and $\mathbf{E}_2$ in Eq. (2) and $\mathbf{C}$ in Eq. (3): i.e.,

$$\mathbf{K}_0 = \int_{x_1} \left(\mathbf{E}_0^{\mathrm{T}} \mathbf{C}^{\mathrm{T}} \mathbf{E}_0\right) A_1 dx_1, \tag{C1}$$

$$\mathbf{K}_1 = \int_{x_1} \left(\mathbf{E}_1^{\mathrm{T}} \mathbf{C}^{\mathrm{T}} \mathbf{E}_0 - \mathbf{E}_0^{\mathrm{T}} \mathbf{C}^{\mathrm{T}} \mathbf{E}_1\right) A_1 dx_1, \tag{C2}$$

$$\mathbf{K}_2 = \int_{x_1} \left(\mathbf{E}_2^{\mathrm{T}} \mathbf{C}^{\mathrm{T}} \mathbf{E}_0 + \mathbf{E}_1^{\mathrm{T}} \mathbf{C}^{\mathrm{T}} \mathbf{E}_1 - \mathbf{E}_0^{\mathrm{T}} \mathbf{C}^{\mathrm{T}} \mathbf{E}_2\right) A_1 dx_1, \tag{C3}$$

$$\mathbf{K}_3 = \int_{x_1} \left(-\mathbf{E}_2^{\mathrm{T}} \mathbf{C}^{\mathrm{T}} \mathbf{E}_1 + \mathbf{E}_1^{\mathrm{T}} \mathbf{C}^{\mathrm{T}} \mathbf{E}_3\right) A_1 dx_1, \tag{C4}$$

and

$$\mathbf{K}_4 = \int_{x_1} \left(\mathbf{E}_2^{\mathrm{T}} \mathbf{C}^{\mathrm{T}} \mathbf{E}_2\right) A_1 dx_1 . \tag{C5}$$

The mass matrix is

$$\mathbf{M} = \int_{x_1} \rho h \left(\boldsymbol{\chi}^{\mathrm{T}} \boldsymbol{\chi}\right) A_1 dx_1 . \tag{C6}$$

Nodal forces (for both internal and external forces) are

$$F_{m1} = \left[N_{11} + M_{11}/R_1\right]_{\text{node } m}, \tag{C7}$$

$$F_{m2} = \left[N_{12} + M_{12}/R_2\right]_{\text{node } m}, \tag{C8}$$

$$F_{m3} = \left[N_{13} + \frac{1}{A_2}\frac{\partial M_{12}}{\partial x_2}\right]_{\text{node } m}, \tag{C9}$$

and

$$F_{m4} = \left[M_{11}/A_1\right]_{\text{node } m}, \tag{C10}$$

where the first index in each component in the point force vector represents node number. Finally, the generalized, distributed force is

$$Q_{mn} = \int_{x_1} \left(q_n \chi_{mn}\right) A_1 dx_1 . \tag{C11}$$

References

(1) Bolton, J. S. and Kim, Y.-J., 2000, "Wave Number Domain Representation of Tire Vibration," Proc. of Inter-Noise 2000, pp. 184-190.

(2) Kim, Y.-J. and Bolton, J. S., 2001, "Modeling Tire Treadband Vibration," Proc. of Inter-Noise 2001.

(3) Kim, Y.-J. and Bolton, J. S., 2002, "Effects of Rotation on the Dynamics of a Circular Cylindrical Shell with Application to Tire Vibration," manuscript submitted to J. Sound Vib.

(4) Cheung, Y. K., 1976, Finite Strip Method in Structural Analysis, Pergamon Press.

(5) Richards, T.L., 1991, "Finite Element Analysis of Structural-Acoustic Coupling in Tyres," J. Sound Vib. 149(2), pp. 235-243.

(6) Brockman, R. A., Champion, J. H., and Medzorian, J. P., 1992, "Finite Element Analysis of Tire Critical Speeds," Computers & Structures 43(3), pp. 581-593.

(7) C.-M. Nilsson and Finnveden, S., 2002, "Tyre Vibration Analysis with Conical Waveguide Finite Elements," Proc. of Inter-Noise 2002.

(8) Keltie, R. F., 1982, "Analytical model of the truck tire vibration sound mechanism," J. Acoust. Soc. Am. 71(2), pp. 359-367.

(9) W. Soedel, 1993, Vibrations of Shells and Plates, 2nd Ed., Marcel Dekker, Inc., New York.

(10) W. Kropp, 1989, "Structure-borne sound on a smooth tyre," Applied Acoustics 26, pp. 181-192.